Journal of Scientific Research and Development 3 (2): 67-75, 2016
Available online at www.jsrad.org
ISSN 1115-7569

An automated ex-utero cord blood collection device using an intelligent framework

K.Z. Tang *, Q.C. Dinh, Y. Zhao

National University of Singapore/Engineering Design and Innovation Centre, Faculty of Engineering, Singapore

Abstract: Hematopoietic Stem Cells (HSCs) have the ability to transform into various forms of cells and thus are able to replace damaged cells or repair body functions. HSCs transplantation has revolutionized the treatment of fatal hematological, immunological and enzyme deficiency diseases over the past 4 decades. Despite the success, up to 45% of patients have no suitable immunologically compatible donors in local and international registries of available donors. One promising source of HSCs is from Umbilical Cord Blood (UCB), which is usually discarded after delivery of babies. Current methods applied for UCB collection are unable to achieve high yield in an automated manner, which also requires sterility and efficiency at the same time. In this project, a multi-axial rotating structure utilizing a two-axial centrifugal force, with accompanying high speed control methodology, is developed. A fuzzy-based control methodology is used for this structure. Simulation and experimental results will be presented to verify the effectiveness of the proposed approach. Analysis as well as recommendations will be given based on test results for future study.

Key words: Fuzzy-based intelligent control; States space control; Control application; Three-dimensional structure

1. Introduction

Umbilical cord blood (UCB) is the blood that remains in the placenta and umbilical cord after the birth of a baby. It is a rich source of stem cells, especially hematopoietic stem cells (HSCs), which can be used in HSC transplantation as a treatment of various diseases such as leukemia, lymphoma and inherited blood disorders (National Institutes of Health, 2011). They could also be used as autologous stem cell rescue in cancer chemotherapy. Recently, UCB has emerged as a new source of HSCs, besides conventional sources such as bone marrow and peripheral blood. Stem cell collection from UCB can eliminate the pain associated with bone marrow retrieval and reduce the overall cost. Moreover, stem cells harvested from UCB have fewer risks of infections, require less human leukocyte antigen (HLA) matching and reduce the risk of graft versus host disease (Gross et al., 2011).

However, the volume of blood collected from the umbilical cord and the placenta is usually limited using conventional methods, about 50 ml (Tan et al., 2012), hence the quantity of HSCs recovered is not high. As the success of HSC transplantations depends heavily on the amount of HSCs used, there is a need to overcome this limitation of UCB collection by extracting more blood from the umbilical cord as well as the placenta.

The umbilical cord is the connection between the fetus and the placenta. It comprises 3 blood vessels: two arteries and a larger vein. The vessels are surrounded and protected by a substance called Wharton's jelly.

The placenta at term usually has a circular shape, with a diameter of 15-20 cm, a thickness of 3 cm at the center and a weight of approximately 500 g (Burton et al., 2012). It comprises two surfaces: the basal plate on the maternal side and the chorionic plate on the fetal side. The umbilical cord is attached slightly eccentrically to the chorionic plate. Between is two plates is a cavity, called the intervillous space, where maternal blood flows through. On the fetal side, there are many villous trees that start from the chorionic plate and branch into the intervillous space. The exchange of nutrients and oxygen occur at the terminal villi, between maternal blood outside the villous trees and fetal blood circulating within the villi. Hence, the two circulations are separated and there is no mixing of maternal and fetal blood. The arteries and veins of the villous trees are branched from the chorionic arteries and veins, which lie in the chorionic plate in a centrifugal manner. Those chorionic arteries and veins are in turn branched from the two umbilical arteries and one umbilical vein, which come out of the placenta through the umbilical cord.

UCB collection has primarily been done using syringe-assisted or gravity-assisted methods (Tan et al., 2007). According to the Singapore Cord Blood Bank, the current clinical procedure is described as follows: After the baby has been delivered, the umbilical cord is clamped and cut, and a needle is then inserted into the umbilical vein and blood flows out to a blood bag by gravity. This process is carried out when the placenta is still inside the uterus and finishes when it is expelled (Singapore Cord Blood

* Corresponding Author.

Bank, 2014). Over the years, a few ex-utero devices have been developed to collect more cord blood even after the delivery of the placenta (Tan et al., 2007) but none of them has performed well enough.

Proposed methodology of an ex-utero approach to collect UCB utilizing 3D centrifugal force

A conceptual design which utilizes centrifugal force is illustrated in Fig. 1. The placenta is put in the funnel 1 with the umbilical cord going through the bottom hole, and the funnel, together with the placenta, is rotated about axis 2 at radius 4. Another rotation about axis 3 takes place at the same time to facilitate the flow of blood.

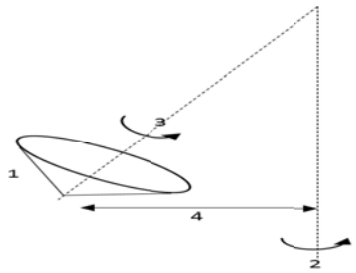

Fig. 1: Conceptual design

1.1. Sectorial view of the placenta

A placenta can be seen as a set of cross sections in which a cross section includes the umbilical cord as illustrated in Fig. 2. Eventually, all of the cross sections, numbered from 1 to *n* will cover the entire placenta as shown in Fig. 3.

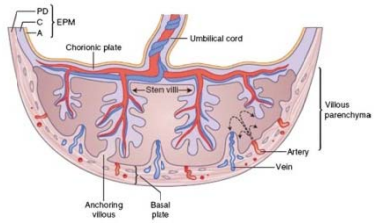

Fig. 2: Cross section of a placenta (Ernst, 2011)

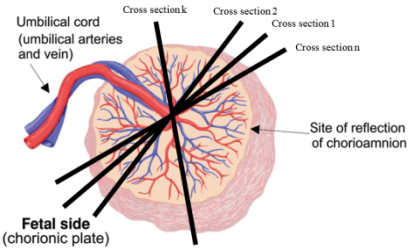

Fig. 3: Cross sections of a placenta (adopted from (Rampersad et al., 2011))

1.2. Force analysis

Due to the rotation and gravity, each point of a cross section experiences a resultant force *F*, in which the magnitude and direction of the resultant force can be controlled by the speed of rotation. Hence, at the cross-sectional area of the placenta that goes through the umbilical cord, the blood inside chorionic vessels that are on the right side of the cross section, as shown in Fig. 4, can be forced out of the placenta through the umbilical cord. Moreover, blood at high-order villi can also be forced out to the stem villi and eventually to the chorionic blood vessels. Since the directions of the villous branches are complicated, the rotation speed can be adjusted to facilitate this process by varying the direction of the force *F*.

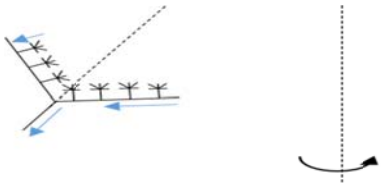

Fig. 4: Placenta during rotation. The arrows indicate expected blood flow

Finally, in order for the whole placenta, i.e. for every single cross section, to experience the same effect, the speed variations of the dual-axial structure have to be performed carefully. One possible advantage of this method over pressure-assisted methods is that the desired force acts directly on the blood whereas in the other scenario, the compression can only affect the blood indirectly through internal "layers" inside the placenta. Furthermore, the entire process can be automated and the placenta stays in the enclosed compartment during the operation, reducing the contact of the object to the external environment thus reducing the risk of cord blood contamination.

1.3. Proposed structure

The proposed hardware of the system is shown in Fig. 5. After delivery, the placenta will be placed in the funnel-like placenta holder and the holder is then connected to the lid to form an enclosed compartment.

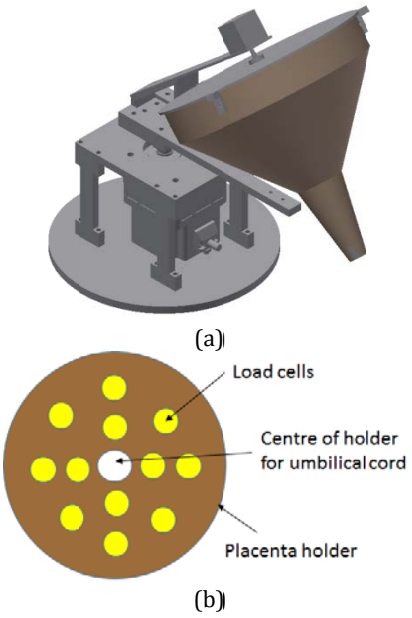

Fig. 5: (a) Proposed structure. (b) Top view of the funnel-like placenta holder from the lid

1.4. Primary rotation

The primary rotation is realized by an AC speed-controlled motor which spins everything attached to its shaft, including the compartment holder and another motor system which will be described later. This motion is the key to the enhanced force acting on the blood and has a magnitude of:

$$|\vec{F}| = \sqrt{(mg)^2 + (m\omega^2 r)^2} = m\sqrt{g^2 + \omega^4 r^2}$$

It is observed that in order to achieve a significant force enhancement compared to sole gravity, the rotation speed should be at least 100 rpm. Furthermore, to ensure safety, it should not be more than 200 rpm. Therefore, the speed of the primary rotation will be in the range of 100-200 rpm.

Also, the direction of the resultant force determines the dimensions of the compartment. As the main focus of this centrifugal enhancement is on the chorionic vessels, which accommodate a lot of cord blood, the design of the compartment will be such that it can align the resultant force with these vessels.

The direction of the resultant force is determined by tanα= (ω^2 r)/g. Taking the speed of 200 rpm (for the largest *F*), the calculated angles at various radii are shown in Table 1.

Table 1: Calculated angles of resultant force *F*

r (cm)	Angle (°)
5	67
10	78
15	82
20	83

Hence, a compartment with such an average angle of 80° is able to align forces at different spots with the chorionic vessels. A recommended dimension of the compartment, i.e. the funnel, is described in Fig. 6.

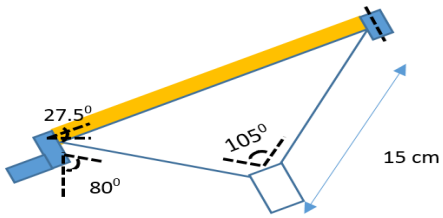

Fig. 6: Recommended compartment dimensions

1.5. Secondary rotation

The purpose of the secondary rotation is to turn the placenta slowly so that every cross section of it can experience the force introduced by the primary rotation. In this design, the secondary motor is being mounted on the rotating platform attached to the shaft of the primary motor and thus requires wireless control. Furthermore, due to the requirement that this secondary motor needs to hold the funnel during the operation of the primary motor and it only turns a bit once in a while, it is suggested that a stepper motor is used to implement this secondary rotation as it can precisely rotate a specified angle and provides a reasonable holding torque that prevents the compartment from unpredictably turning during the operation.

2. Intelligent framework for fuzzy inference and control

In this paper, an intelligent framework that is able to configure. the centrifugal effect for each of the two axes that is customized to each run based on the weight and size of the placenta is developed.

Utilizing a fuzzy operation, a self-adapting fuzzy approach that can be precisely adapted to the dynamic and multi-criteria learning environment is developed. The key idea in the proposed approach is to associate the data from the array of sensors in the system with inferred attributes. The attributes are associated with the characteristics (i.e. size and weight) of the individual placenta. These attributes are fuzzy variables (i.e., $x_i \in [0, 1]$, i=0, 1, …, n) computed from a fuzzy operation on a combination of variables which are expected to influence the rotational speeds of the two axes. Decisions taken by the intelligent system will be driven primarily by these attributes.

2.1. Takagi and Sugeno's fuzzy rules

The attributes are inferred from a Takagi and Sugeno type of fuzzy inference. Consider the following p rules governing the attribute of the kth individual:

$$IF\ x^i_{k1}\ is\ F^i_1 \otimes \ldots \otimes x^i_{km_i}\ is\ F^i_{km_i}\ THEN\ u^i_k\ is\ \alpha^i,\ i = 1 \ldots p \quad (1)$$

with ($\sum_{i=1}^{p} \alpha^i = 1$), where F^i_j are fuzzy sets, $x^i = (x^i_{k1}, \ldots, x^i_{km_i})^T \in U$ are the input linguistic variables identified to affect the learning characteristic for rule i, $\otimes$ is a fuzzy operator which combine the antecedents into premises, and u^i_k is the crisp output for rule i. α^i is the scaling factor for rule i reflecting the weight of the rule in determining the final outcome.

In the application, x^i_{kj} is the linguistic variable and F^i_j is the fuzzy set. The value of the *Attribute* is then evaluated as a weighted average of the u^i`s:

$$Attribute_k = \frac{\sum_{i=1}^{p} w^i_k u^i_k}{\sum_{i=1}^{p} w^i_k} \quad (2)$$

Where the weight w^i_k implies the overall truth values of the premise of rule i for the input and is calculated as:

$$w^i_k = \prod_{j=1}^{m_i} \mu_{F^i_{kj}} x^i_{kj} \quad (3)$$

Under this framework, it is relatively easy to include additional criterion for decision. The procedure will involve setting the membership functions for the criterion, formulating the additional fuzzy rules required, and adjusting the scaling parameters, i.e., α's as mentioned in (1), to reflect

the relative weight of the new criterion over the existing ones.

Development of Scheduled control methodology

To provide the initial rotational speeds of the different axes, the control parameters of the two axes have to tune so that the controller could schedule the respective settings for the actuators.

3. System identification

System model needs to be obtained to design the controller. Suppose the system transfer function is *H(s)*, therefore for input *V(s)* and output *Y(s)*, the following equation holds.

$$\frac{\mathrm{Y(s)}}{\mathrm{V(s)}} = \mathrm{H(s)}$$

If the input is an impulse, *V(s)* = 1, then the output transfer function will be the system transfer function, i.e. *Y(s) = H(s)*. The impulse input can be approximated through controller output, as switching on and off power supply manually will introduce a relatively big error. The motor speed response is fed into LabVIEW through encoder output. Different pulse durations are tested out to observe the system performance. From the relation between control voltage and output speed, the system gain will be the same as the curve gradient, and this can be used as a benchmark for system identification result.

For DC motor with a viscous friction model, that is, the friction torque is proportional to shaft angular velocity, the transfer function between control voltage (V) and output speed (rad/s) is:

$$\mathrm{H(s)} = \frac{\dot{\theta}(\mathrm{s})}{\mathrm{V(s)}} = \frac{\mathrm{K}}{(\mathrm{Js}+\mathrm{b})(\mathrm{Ls}+\mathrm{R})+\mathrm{K}^2}$$

Where K(V/rad/sec) is electromotive force constant, J(kg*m2) is moment of inertia, b(N*m*s) is motor viscous friction constant, L(H) is electric inductance, and R(ohm) is electric resistance.

Given the system transfer function has the model $\frac{\mathrm{K}}{(\mathrm{Js}+\mathrm{b})(\mathrm{Ls}+\mathrm{R})+\mathrm{K}^2}$, the system output should be the Inverse Laplace Transform of the transfer function, i.e. having the form of $\mathrm{A} * \mathrm{e}^{-\mathrm{Bt}} * \sin(\mathrm{Ct})$. Parameters A, B, C are obtained using curve fitting analysis with software Origin9.0. Here the speed with unit rpm is used, because change in unit results in change in Parameter A, B, C value, and the general formula will not change.

3.1. Primary motor

For primary motor, pulses with duration from 0.05 second to 1 second are applied, and the speed response is captured by LabVIEW. Theoretically, the input control signal should have less duration to simulate impulse signal. However, in reality, if the duration is too small, the system will not respond at all. After the speed response is obtained, curve fitting is applied and the results of A, B, C are tabulated in Table 2. In addition, the system gain is also calculated to verify the correctness of the result. It equals to transfer function value when s = 0. The adjusted coefficient of determination (R2), which measures how well the regression line approximates the real data points, is also included. R2 of 1 indicates that the regression line perfectly fits the data.

The system gain is nearest to the correct value with pulse duration being 0.75 second, and Parameters A, B, C are obtained by taking the average of experiments with 0.75 second.

A = 159.377, B = 2.3463, C = 1.5298

The Laplace Transform of $\mathrm{A} * \mathrm{e}^{-\mathrm{Bt}} * \sin(\mathrm{Ct})$ is $\mathrm{A} * \frac{\mathrm{C}}{(\mathrm{s}+\mathrm{B})^2+\mathrm{C}^2}$. With A = 159.377, B = 2.3463, C = 1.5298, impulse input with an amplitude of 1, system model of primary motor is $\frac{243.8208}{s^2+4.6926*s+7.8456}$. The system gain is $\frac{243.8208}{7.8456}$ = 31.0775, which is quite close to the curve gradient 31.061.

3.2. Secondary motor

Same as primary motor, for secondary motor, pulses with duration from 0.2 second to 1.2 second are applied, and the speed response is captured by LabVIEW. When the pulse duration is smaller than 0.2 second, the motor has no response at all. After the speed response is obtained, curve fitting is applied and the results of A, B, C are tabulated in Table 1. Same as before, the system gain and the adjusted coefficient of determination (R2) are also included.

From Table 1, when the pulse duration increases from 0.2 second to 1.2 second, the system gain increases from around 4 to 66. It gets closer to the correct value. More importantly, R2 increases and eventually reaches 0.99961, which means the curve fitting is more accurate when the pulse duration increases. The short pulse signal probably cannot drive the motor too much, so the speed response is less accurate. The system gain is nearest to the correct value with pulse duration being 1.2 second, and Parameters A, B, C are obtained by taking the average of experiments with 1.2 second.

A = 150.6835, B = 1.125355, C = 0.84009

The Laplace Transform of $\mathrm{A} * \mathrm{e}^{-\mathrm{Bt}} * \sin(\mathrm{Ct})$ is $\mathrm{A} * \frac{\mathrm{C}}{(\mathrm{s}+\mathrm{B})^2+\mathrm{C}^2}$. With A = 150.6835, B = 1.125355, C = 0.84009, impulse input with an amplitude of 1, system model of primary motor is $\frac{126.5877}{s^2+2.25071*s+1.9722}$. The system gain is $\frac{126.5877}{1.9722}$ = 64.186, which is quite close to the curve gradient 64.143.

Simulation

With the system model derived, the next objective is to simulate the system and obtain the closed-loop controller gain as well as estimator gain. The settling time, overshoot, as well as the steady state gain between output and reference are the criteria for selecting the closed-loop controller gain and estimator gain. The criteria are specified as below:

- Steady state gain between output and reference: 0dB;
- Settling time: not more than 2 seconds;

➢ Overshoot: smaller than 5%.

For these two motors, two structures are designed: without integral action and with integral action. In this project, motor speed (state variable x_1) is obtained through encoder output, whereas the motor acceleration (state variable x_2) cannot be obtained directly. It can either be the derivative of motor speed, or estimator can be utilized to estimate its value.

3.3. Without integral action

The control structure is drawn out in Fig. 7. Estimator can estimate the value of velocity and acceleration, and these two parameters are feedback to control signal "u" with feedback gain K. The closed-loop gain is no longer the original plant gain. Parameter Ks is added to make the entire system gain being 1 so that the steady-state gain between output and reference is 0 dB. This control structure is quite simple and straightforward; however, the plant model needs to be accurate for perfect control. If the plant model is not very precise, the system gain calculated and subsequently parameter Ks implemented will not be very accurate.

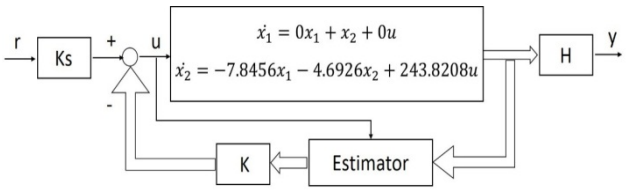

Fig. 7: Control Structure without Integral Action

LabVIEW is used to simulate the system and obtain feedback gain K and estimator gain by observing closed-loop step response. For the primary motor, the system is both observable and controllable. The controller poles are set to be -10 ± 5i so that the closed-loop step response has no overshoot and quick response.

3.4. With integral action

The control structure is drawn out in Fig. 8. Other than estimator and feedback gain K, the difference between output velocity and set-point is integrated with integration gain K_I, and fed into control signal "u". To construct the state-space model, there is a new state variable X_I added, and $\dot{x}_I = y - r$.

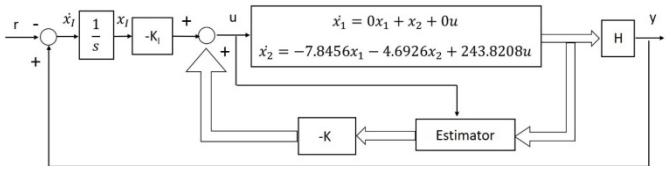

Fig. 8: Control Structure with Integral Action

Using this method, it has the advantage of making output follows reference exactly and eliminating disturbance. Because $\dot{x}_I = y - r$, in the long run, $\dot{x}_I$ becomes zero so output is the same as reference.

The estimator pole should be 2-6 times of feedback pole to make sure the estimator error decays fast and thus apply the correct feedback. ω_o is the design parameter based on the given plant model. The feedback gain as well as estimator gain is obtained through simulation in MatLab.

For the primary motor, different simulation results are tabulated in Table 2. It can be seen that when ω_o increases, feedback gain and closed-loop bandwidth increase. Overshoot does not change and settling time decreases. It means with large feedback gain, the system responses faster. However, the settling time is not significantly improved. The design parameter needs to be implemented to verify its feasibility.

Table 2: Simulation results for primary motor, with integral action

ω_o	KI	K1	K2	Closed-loop bandwidth (rad/s)	Overshoot (%)	Settling Time (s)
2	0.03281	0.00828	0.00071	1.4217	0.756	2.53
3	0.11074	0.05885	0.01069	2.1325	0.756	1.69
4	0.26249	0.12965	0.02067	2.8433	0.756	1.27

4. Experimental study

Based on the simulation results above, controller gains are implemented on primary and secondary motor in a closed-loop system to test their feasibility. During implementation phase, the controller is first implemented using state-space design methodology (integral and no integral). It follows these steps:

Select the Sampling Period → Tune and Determine Control Design Parameter → Verify Performance with Different Loads

The state-space design methodology is then compared with feed forward with PI (Proportional and Integral) control methodology. Analysis is given and conclusion can be drawn from there.

During fine-tuning of the proposed system, there is a shortage of placenta samples. Water bag together with blood bag is used to substitute placenta. Water bag is filled with different water volume, and blood bag tube is inserted into water bag. The connection is fasted by a balloon.

4.1. Primary motor

4.1.1. With integral action

The implementation follows the design structure of Fig. 8.

4.1.2. Without integral action

The implementation follows the design structure of Fig. 7. Previous simulation result indicates the controller gain to be -10 ± 5i. Therefore, this control structure is simulated again using, and the results are tabulated in Table 3. The selection of closed-loop

pole locations follows Bessel Prototype Table Methodology.

Table 3: Simulation results for secondary motor, without integral action

ω_o	Ks	K1	K2	Closed-loop bandwidth (rad/s)	Overshoot (%)	Peak Time (s)
3	0.03691	0.004733	0.002065	2.3544	0	2.09
4	0.06562	0.033441	0.009168	3.1392	0	1.57

When ω_o = 3 rad/s, it is found that the steady-state gain between output and set point is not 0dB (Fig. 4.17). It is because the system identification is not hundred percent accurate, so the parameter Ks used for controlling overall system gain is not very accurate. Ks is adjusted accordingly to be 0.043 for ω_o = 3 rad/s, and 0.075 for ω_o = 4rad/s, and the implementation results for simulation above is shown in Fig. 9.

4.2. Secondary motor

For secondary motor, state-space method is not suitable. The motor and placenta holder are in a tilted position, therefore any load added is also tilted. When the motor turns, the load will move up and down, bringing a disturbance to the system. The motor speed without control is oscillatory itself. This makes the system identification of the model inaccurate. Given previous good performance of feedforward with PI control, this method is adopted for secondary motor. Based on the control voltage and speed relation in Fig. 3.11, the block diagram is the same as primary motor (Fig. 4.25). The final proportional gain is 0.005, and the integral gain is 0.003.

4.3. Performance comparison of overall system

To verify precession effect as well as to compare designed approach with gravity-assisted method, five experiments are conducted in total as summarized in Table 4.

Table 4: Summary of five experiments conducted

Experiment Number.	Experiment Design Description
1	Vary primary speed with secondary speed constant to verify precession effect. Time taken is 40 seconds. Volume of fluid collected is measured.
2	Vary secondary speed with primary speed constant to verify precession effect. Time taken is 40 seconds. Volume of fluid collected is measured.
3	Vary both primary and secondary speed with fixed speed ratio to obtain optimal speed combination. Time taken is 40 seconds. Volume of fluid collected is measured.
4	To compare 3D centrifugal method and gravity-based method, time taken for all the water to flow out is recorded. Volume of fluid collected ranges from 500-700ml.
5	To compare 3D centrifugal method and gravity-based method, Volume of fluid collected in 30 seconds is recorded.

To determine the influence of primary rotation speed and secondary rotation speed as well as verifying the precession effect, two sets of experiments are conducted by considering only one factor at a time. The first is varying primary rotation speed with secondary speed being constant, and the second is to change secondary speed while maintaining the primary rotation speed. Water is used to simulate the actual UCB using mock placentas. Water (600ml) is contained in a water bag, and it is collected using clinical blood bag.

The primary speed and secondary speed are set in programming. The water sample collected is measured after 40 seconds. The results are summarized in the following tables and graphs (Table 4 and 5, Fig. 9 and 10).

According to the two graphs (Fig. 9 and 10), it can be seen when the speed ratio is 3.472, the collected volume is most. This is in accordance with previous theory about precession effect, which says when the processional forcing is at the resonant frequency of the fundamental inertial mode, the fluid inside responses strongest. The resonant frequency of the fundamental inertial mode is obtained when the speed ratio is 3.472.

Table 5: Experiment result by varying primary speed with secondary speed fixed

Primary Speed(rpm)	Secondary Speed(rpm)	Time(s)	Volume(ml)	Speed Ratio
12.5	25	40	275	0.5
27.5	25	40	300	1.1
42.5	25	40	330	1.7
47	25	40	380	1.88
57.5	25	40	330	2.3
75	25	40	370	3
86.8	25	40	410	3.472
95	25	40	385	3.8

Table 6: Experiment result by varying secondary speed with primary speed fixed

Primary Speed(rpm)	Secondary Speed(rpm)	Time(s)	Volume(ml)	Speed Ratio
75	60	40	330	1.25
75	55	40	340	1.363636
75	50	40	360	1.5
75	45	40	375	1.677777
75	40	40	400	1.875
75	35	40	300	2.142857
75	30	40	350	2.5
75	25	40	355	3
75	21.6	40	445	3.472222
75	20	40	400	3.75
75	15	40	380	5

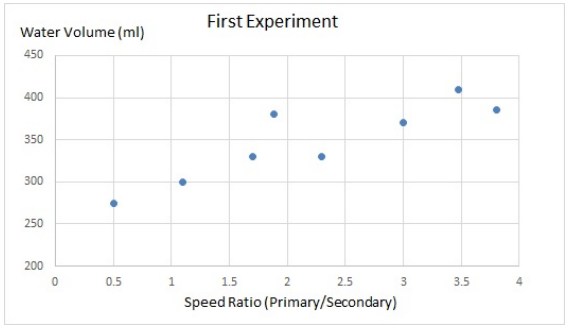

Fig. 9: Experiment result by varying primary speed with secondary speed fixed

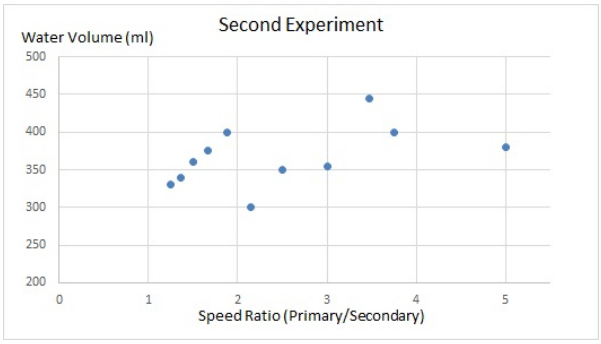

Fig. 10: Experiment result by varying secondary speed with primary speed fixed

The analysis of secondary rotation is as shown in Fig. 11. One component of the support force acts as the centrifugal force. However, with larger centrifugal force to drive the water into the middle section of the funnel, the other component of the support force F1 also becomes larger in magnitude, which counteracts the gravitational force and makes water more difficult to flow downwards. If the speed of secondary rotation is large enough to the extent that F1 can counteract the gravitational force completely, the water inside the funnel will not flow out at all. This explains why water volume collected does not increase continuously with secondary rotation speed.

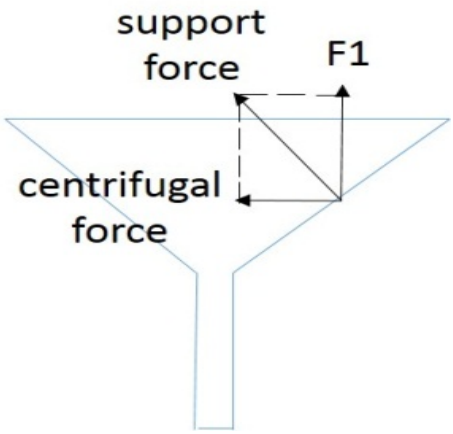

Fig. 11: Force Diagram of Secondary Rotation

For primary rotation, the speed will affect the water flow in a similar way as secondary motor. At the same time, the tilting angle of placenta holder also has an influence. The tilting angle is 50 degree as designed earlier, given primary rotation speed being 75rpm. Experiments are further conducted to determine the optimal primary rotation speed. The primary and secondary speed ratio is fixed to be 3.472. Results are shown in the Table 7.

Table 7: Experiment result with speed ratio fixed to be 3.472.

Primary Speed(rpm)	Secondary Speed(rpm)	Time(s)	Volume(ml)	Speed Ratio
57.5	16.56	40	395	3.472
75	21.6	40	445	3.472
86.8	25	40	410	3.472
90	25.92	40	350	3.472

The optimal speed is obtained when primary motor is 75rpm. At this speed, the force direction is the same as placenta holder tiling angle. To sum up, the primary rotation speed is 75rpm, and the secondary rotation speed is 21.6rpm.

After obtaining the optimal speed, experiments are further conducted to compare the proposed approach with gravity-based method. Water sample is again used to replace blood due to lack of available placentas. Two sets of experiments are conducted.

The first experiment is to determine how much time it takes for normal placentas weighing about 500-700g to allow all the UCB to flow out. Water samples of mock placentas weighing from 500-700g, i.e. 500-700ml, are tested using gravity-based method and 3D centrifugal method respectively. For each case, two tests are taken to minimize human error. Amount of time taken (seconds) for all the water to flow out are tabulated in Table 8 and drawn in Fig. 12.

Table 8: Experiment result of gravity-based method and 3d centrifugal method

Water Volume (ml)	Gravity-based Method			3D Centrifugal Method		
	Test 1	Test 2	Average	Test 1	Test 2	Average
500	77	68	72.5	43	45	44
550	83	75	79	46	44	45
600	80	85	82.5	46	50	48
650	88	90	89	48	52	50
700	89	94	91.5	50	52	51

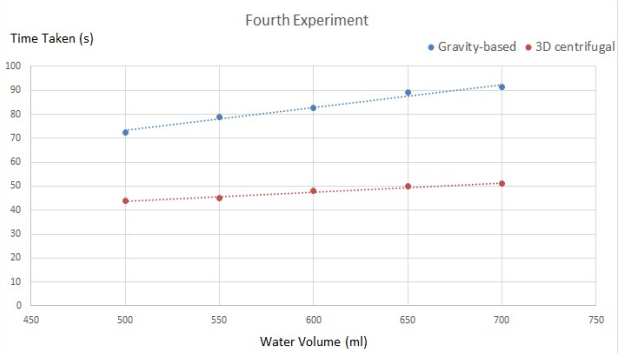

Fig. 12: Experiment result of gravity-based method and 3d centrifugal method

Firstly, for same amount of water to flow out, amount of time taken using 3D centrifugal method is significantly less than that using gravity-based method. This applies to different water volume from 500-700ml. This proves the effectiveness of proposed structure and its promising future to replace gravity-assisted method. Secondly, amount of time taken and water volume follows a rough linear relationship. There is minor error during experiments. For example, for the cases 550ml and 600ml of water, the first tests using 3D centrifugal method take the same time. This is because during experiment, it is quite subjective to determine whether all of the water flows out. The same experiment should be done with placentas to estimate how much time it takes for blood collection.

The second experiment is to compare amount of water flow out within same period of time. Because during last experiment, it takes more than 40 seconds for water to flow out, here the time is chosen as 30 seconds. Similarly, water samples weighing from 500-700g, i.e. 500-700ml, are tested using gravity-based method and 3D centrifugal method respectively. For each case, two tests are taken to minimize human error. Amount of water flow out (ml) in 30 seconds are tabulated in Table 9.

Table 9: Experiment result of gravity-based method and 3d centrifugal method, time 30 seconds

Water Volume (ml)	Gravity-based Method			3D Centrifugal Method		
	Test 1	Test 2	Average	Test 1	Test 2	Average
500	225	235	230	340	330	335
550	230	215	222.5	335	345	340
600	220	230	225	315	340	327.5
650	240	240	240	325	345	335
700	230	235	232.5	350	345	347.5

Firstly, with different initial water volume, amount of water flowing out in 30 seconds does not vary a lot, which means initial water volume has little effect in water flow rate. Secondly, amount of water collected using 3D centrifugal method is more than that using gravity-based method, which again proves the effectiveness of proposed approach.

In summary, the optimal speeds are 75rpm and 21.6 rpm for primary rotation and secondary rotation. The proposed 3D centrifugal method is verified to be more efficient than gravity-assisted method currently adopted in hospitals.

5. Conclusions

With the development of such a device, a very real market need (shortage of HSC transplants) can be met. By providing for more HSC transplants, this device would have indirectly improved global health and patient wellbeing. A fuzzy-based control methodology is proposed for this structure. With this framework in place, a machine learning mechanism can be invoked to allow the system to auto-tune the parameters to suit each placental condition. Simulation and initial experimental results are presented to verify the effectiveness of the proposed approach.

References

G. A. Gross, T. Nguyen and L. Meints, "Umbilical Cord Blood Banking," in The Placenta. From Development to Disease, 1st ed., Blackwell Publishing Ltd., 2011, pp. 321-326.

G. J. Burton, C. P. Sibley and E. R. M. Jauniaux, "Placental Anatomy and Physiology," in Obstetrics. Normal and Problem Pregnancies, 6th ed., Saunders, 2012, pp. 3-22.

K. K. Tan, K. Z. Tang and S. Huang, "Devices for Umbilical Cord Blood Collection," Recent Patents on Engineering, vol. 1, no. 1, pp. 89-94, 2007.

K. K. Tan, K. Z. Tang, A. S. Putra, X. Pu, S. Huang, T. H. Lee, S. C. Ng and L. G. Tan, "An auto-perfusing umbilical cord blood collection instrument," ISA Transactions, vol. 51, no. 3, pp. 420-429, 2012.

L. M. Ernst, "Placenta," in *Color Atlas of Fetal and Neonatal Histology*, Springer, 2011, pp. 363-388.

National Institutes of Health, U.S. Department of Health and Human Services, "5. Hematopoietic

Stem Cells," 20 January 2011. [Online]. Available: http://stemcells.nih.gov/info/scireport/pages/chapter5.aspx. [Accessed 30 March 2014].

R. Rampersad, M. Cervar-Zivkovic and D. M. Nelson, "Development and Anatomy of the Human Placenta," in *The Placenta: From Development to Disease*, H. Kay, D. M. Nelson and W. Y., Eds., Wiley-Blackwell, 2011, pp. 19-26.

Singapore Cord Blood Bank, "Cord Blood Collection," [Online]. Available: http://www.scbb.com.sg/donate/collection/Pages/Home.aspx. [Accessed 30 March 2014].